JOURNAL OF PROPULSION AND POWER
Vol. 24, No. 4, July–August 2008

Experimental and Numerical Investigation of n-Heptane/Air Counterflow Nonpremixed Flame Structure

P. Berta and S. K. Aggarwal*
University of Illinois at Chicago, Chicago, Illinois 60607
Ishwar K. Puri
Virginia Polytechnic Institute and State University, Blacksburg, Virginia 24061
and
S. Granata, T. Faravelli, and E. Ranzi
Politecnico di Milano, 20100 Milan, Italy

DOI: 10.2514/1.33025

An experimental and numerical investigation of prevaporized n-heptane nitrogen-diluted nonpremixed flames is reported. The major objective is to provide well-resolved experimental data regarding the structure and emission characteristics of these flames, including profiles of major species (N_2, O_2, C_7H_{16}, CO_2, CO, H_2), hydrocarbon intermediates (CH_4, C_2H_4, C_2H_2, C_3H_x), and soot precursors (C_6H_6). A counterflow flame configuration is employed, because it provides a nearly one-dimensional flat flame that facilitates both the detailed measurements and simulations using comprehensive chemistry and transport models. The measurements are compared with predictions using a detailed n-heptane oxidation mechanism that includes the chemistry of NO_x and polycyclic aromatic hydrocarbon formation. The measurements are compared with predictions using a detailed n-heptane oxidation mechanism that includes the chemistry of NO_x and polycyclic aromatic hydrocarbon formation. Measurements and predictions exhibit excellent agreement for temperature and major species profiles (N_2, O_2, n-C_7H_{16}, CO_2, CO, and H_2), reasonably good agreement for intermediate species (CH_4, C_2H_4, C_2H_2, and C_3H_x), but significant differences with respect to benzene profiles. Consequently, the benzene submechanism was synergistically improved using pathway analysis and measured benzene profiles.

Introduction

LIQUID fuels are an important energy source due to their widespread use in various propulsion and energy-conversion applications such as internal combustion engines and gas turbine combustors. The various physical and chemical processes involved in liquid-fuel combustion have very complex interactions. In most practical devices, the liquid fuel is introduced into the combustion chamber in the form of a spray that consists of droplets that have a wide size and velocity distribution, resulting in disparate vaporization rates. Therefore, to avoid the complexities associated with the droplet/vapor transport and nonuniform evaporation processes, a fundamental investigation of liquid-fuel combustion in an idealized configuration that precludes vaporization is very useful. Also, although most practical liquid fuels are blends of several components, the investigation of an idealized fuel surrogate such as n-heptane can provide useful information about the combustion chemistry of heavier-hydrocarbon liquid fuels. In addition, n-heptane is also a reference fuel in the definition of the octane number and its oxidation chemistry has been extensively investigated [1–22].

Several investigations dealing with n-heptane flames have been reported in recent years. The combustion of n-C_7H_{16} has been investigated with reduced chemical mechanism for analyses of burning velocities [1], the structure and extinction of nonpremixed flames [2–4], and liquid-pool flames [5–7]. Semidetailed and detailed chemistry models have also been used to analyze n-C_7H_{16} combustion in various flame configurations [8–11]. A detailed mechanism describing C_7 pyrolysis and oxidation has been developed using extensive experimental data from a variety of experiments [12]. Experimental investigations of n-C_7H_{16} combustion have been performed using jet-stirred and plug-flow reactors [8,13], liquid pools [14–16], and droplets [17,18] and to determine premixed burning velocities [19]. In spite of the many previous investigations [20–22], there is a paucity of detailed measurements in well-characterized n-heptane flames, especially regarding the distribution of intermediate species such as C_1–C_6 hydrocarbons, which are important from the perspective of validating the detailed reaction mechanisms and characterizing NOx and soot-formation pathways. Moreover, a fundamental understanding of n-heptane flames under a wide range of conditions can assist in the design and optimization of various liquid-fueled combustion systems with respect to efficiency and overall emissions of NOx and particulate matter.

Gaseous polycyclic aromatic hydrocarbon (PAH) species and soot particles are undesirable pollutants because they reduce efficiency and have a detrimental health impact, particularly on the cardiopulmonary system [23]. Soot particles are formed inside hydrocarbon flames through the pyrolysis of hydrocarbon molecules and subsequent heterogeneous processes that are very complex [24,25]. However, because soot is formed through large benzene and larger PAH molecules, characterizing these species accurately is important to further improve the PAH formation chemistry. Seiser et al. [20] investigated the extinction of nitrogen-diluted n-heptane/air counterflow nonpremixed flames. Li and Williams [21] examined the structure of similar partially premixed flames But when the liquid fuel was introduced as a spray. Berta et al. [22,26] characterized the structure and emission characteristics of prevaporized n-heptane partially premixed flames. Liu et al. [27] reported a numerical study of the effect of strain rate on the transient autoignition of nonpremixed n-heptane at high pressures in a counterflow configuration.

Our primary objective is to provide useful experimental data for nitrogen-diluted n-heptane nonpremixed flames in a configuration that removes the complexities associated with droplet transport and vaporization. We measured temperature and species (including

Received 27 June 2007; revision received 18 February 2008; accepted for publication 14 March 2008.

*Professor, Department of Mechanical and Industrial Engineering; ska@uic.edu (Corresponding Author).

C_1–C_6 and PAHs) concentration profiles for prevaporized n-heptane nonpremixed flames for different strain rates and nitrogen dilution. These flames have also been simulated using a detailed reaction mechanism that also considers soot precursors such as acetylene and benzene [12,28–30]. An improved mechanism to predict benzene and higher-PAH species is proposed based on the measurements and a sensitivity analysis.

Experimental Apparatus

A schematic diagram of the experimental setup in which the counterflow flames were established is presented in Fig. 1. The separation distance between the counterflow nozzles was varied from 10 to 15 mm. Both nozzle diameters were 27.38 mm. A mixture of prevaporized n-heptane and nitrogen fuel was introduced from the bottom nozzle. A nitrogen curtain was established through an annular duct surrounding the fuel jet to isolate the flames from ambient disturbances. This nitrogen and combustion products were vented and cooled through another annular duct around the oxidizer nozzle. The velocities of the two streams define the global strain rate [31]

$$a_g = \frac{2|V_O|}{L}\left(1 + \frac{|V_F|}{|V_O|}\sqrt{\frac{\rho_F}{\rho_O}}\right)$$

and were chosen to satisfy the momentum balance $\rho_O V_O^2 = \rho_F V_F^2$, where ρ represents density; V is the gas velocity; subscripts O and F refer to the oxidizer and fuel nozzles, respectively; and L is the separation distance between the two nozzles.

The oxidizer was air at room temperature and the fuel stream consisted of mixtures of nitrogen and prevaporized n-heptane. The fuel nozzle was heated and its temperature was controlled to maintain the fuel-containing stream at a 400-K temperature at the burner exit. The N_2/n-heptane mixture was formed in a prevaporizer, which was an electrically heated stainless steel chamber. The desired mass flow rate of n-heptane into the prevaporizer was maintained by a liquid pump while gaseous nitrogen was introduced through the chamber bottom. Approximately three-quarters of the chamber was filled with glass beads to impede the flow, thereby increasing its residence time and thus enhancing the heat transfer to the liquid fuel. The temperature of the fuel-vapor/gaseous-nitrogen mixture exiting the chamber was monitored by a thermocouple.

Temperature profiles of various flames were measured using a Pt/Pt-13%Rh thermocouple with a spherical bead diameter of 0.25 mm and a wire diameter of 0.127 mm. The measured values were corrected for radiation heat losses from the bead, assuming a constant emissivity of 0.2 and a Nusselt number of 2.0 [20]. The uncertainty in temperature measurements was less than 100 K. Species-concentration profiles were measured using a Varian CP-3800 gas chromatograph. Samples were drawn from the flame with a quartz microprobe that had a 0.34-mm tip diameter and 0.25-mm tip orifice. Constant vacuum was applied at the end of the line through a vacuum pump. The line carrying the sample to the gas chromatograph was made of fused silica and was heated to prevent condensation. A portion of the sample was injected into a Hayesep DB 100/120 packed column connected to a thermal conductivity detector to measure light gases (up to C_2H_4), and another portion was injected into a Petrocol DH capillary column that was placed inline with a flame-ionization detector to obtain hydrocarbon distributions up to C_7H_{16}. The temperature in the gas-chromatograph oven was gradually increased to minimize the analysis time. The temperature and pressure in the sampling loops were controlled to ensure that the same volume of gas was sampled for each analysis. The chromatogram peaks were converted into mole fractions with calibration constants that were obtained separately for every species from known standards. Water mole fractions were obtained through a mass balance of hydrogen atoms. Relative experimental errors associated with gas-chromatograph readings were within 10%.

Reaction Mechanism

The reaction mechanism used in this study consists of the high-temperature reactions of a more comprehensive model that was previously developed and tested against a wide range of experimental data for different fuels [28,32]. Because of the hierarchical modularity of the mechanistic scheme, this model is based on a detailed submechanism of C_1–C_4 species. Assuming analogy rules for similar reactions, only a few fundamental kinetic parameters are required for the progressive extension of the scheme toward heavier species. The resulting kinetic model of hydrocarbon oxidation from methane up to n-octane consists of about 170 species and 5000 reactions.

We selected this mechanism for our simulations because the subset of n-heptane oxidation reactions included in it has been extensively tuned by using experimental measurements for pure pyrolysis conditions, oxidation in jet-stirred and plug-flow reactors, and shock tube experiments [12]. Moreover, a relatively detailed model for PAHs that are soot precursors is contained in the mechanism. The formation of the first aromatic rings by the C_2 and C_4 chemistry and by the resonantly stabilized radicals such as propargyl and cyclopentadienyl (C_3H_3 and C_5H_5) has been carefully investigated [29,32]. Further growth of PAH species up to coronene ($C_{24}H_{12}$) is also modeled through the well-known hydrogen-abstraction/carbon-addition (HACA) mechanism [33], which has been extensively validated for counterflow flames burning a variety of fuels [34]. The main consumption reactions of aromatics and PAHs are H-abstraction reactions by H and OH radicals. The high-temperature reactions have been validated against substantial experimental data [28,29,32].

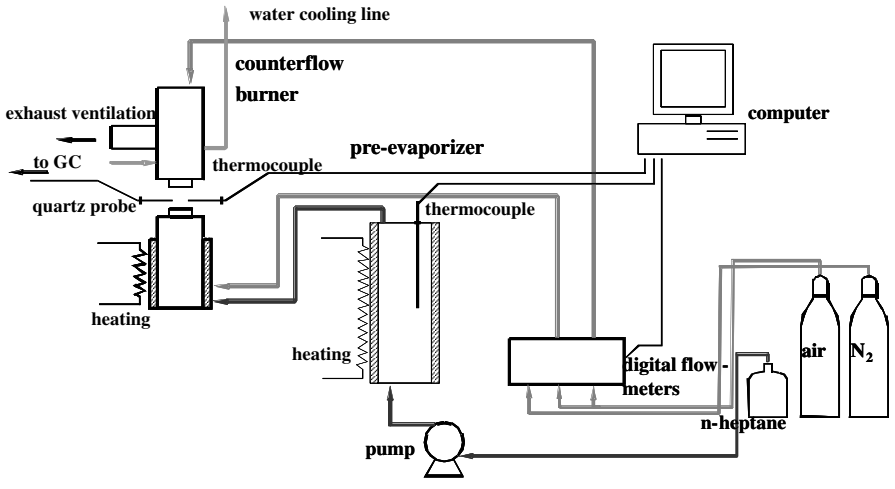

Fig. 1 Schematic diagram of the experimental apparatus.

Table 1 Operating conditions in terms of strain rate, nitrogen dilution (on a percent mole basis), and nozzle-separation distance for the cases investigated numerically and experimentally

Flame	Strain rate, s^{-1}	N_2 dilution, %	Nozzle separation, cm	V_O, cm/s	T_O, K	V_F, cm/s	T_F, K
A1	150	85	1	37.50	300	32.52	400
A2	100	88	1.5	37.45	300	31.93	400
A3	50	90	1	12.57	300	10.98	400
B1	77	50	1	19.07	300	13.11	400

Numerical simulations of counterflow flames were performed using the opposed diffusion flame (OPPDIF) code [35]. The code was modified to handle the complex reaction mechanism. The radiative heat transfer was modeled using an optically thin gas assumption, with CO_2, H_2O, CO, and CH_4 being the participating gaseous species. Further details are provided in [36,37]. The soot radiation is not included because the present study considers flames with moderate strain rates and significant nitrogen dilution in the fuel stream. This is further confirmed by the agreement between the measured and predicted peak flame temperatures. Most thermodynamic properties were obtained from Burcat and McBride [38] and unavailable properties were estimated using the group additivity and difference methods [39]. Transport properties were obtained from the CHEMKIN database [40] wherever available, and unavailable data were deduced through analogy with known species.

Results and Discussion

We performed a detailed parametric investigation to characterize the effects of strain rate and nitrogen dilution on the structure and emission of n-heptane/air nonpremixed flames. We selected four of the cases that were investigated to characterize the flame structures for which the operating conditions in terms of strain rate, nitrogen dilution, and nozzle-separation distance are reported in Table 1. flame A1 corresponds to a strain rate of 150 s^{-1} and a nitrogen dilution of 85%, which are the conditions of Seiser et al. [20]. Their results were used for validation purposes. Flame B1 has a strain rate of 77 s^{-1} and a nitrogen dilution of 50%. It is noteworthy that flame A1 is nearly nonsooting, whereas flame B1 is relatively more sooting.

Figure 2 presents digital images of flames A1 and B1 obtained for the same exposure conditions. Several differences are observed. The thickness of flame A1 is smaller, due to its larger strain. It has a bright blue color that is typical of CO oxidation. Flame B1 is thicker and exhibits an orange-red zone that is indicative of pyrolysis and soot-formation reactions. Although the soot formation is observable in this flame, it is not large enough to present difficulties for the gas sampling technique.

The measurements for flame A1 were compared with those reported by Seiser et al. [20]. Apart from small differences in the concentration profiles of minor species, which are attributed to differences in the experimental methods and associated errors, there was good agreement between the two measurement sets with respect to temperature and species mole fraction profiles. There was also good agreement with respect to the spatial shift observed between the measured and computed temperature profiles in the two studies.

Flame A1

Flame B1

Fig. 2 Digital images of two N_2-diluted nonpremixed n-heptane flames.

Figure 3 presents a comparison between the predicted and measured temperature and species-concentration profiles for flames A1 and B1. The predictions are based on the numerical and chemistry models described in the preceding section. Results for flame A1 are shown on the left and those for case B1 are on the right. The predicted velocity profiles are also shown in the figure to locate the stagnation plane. Except for a slight misalignment, there is good agreement between the numerical and experimental profiles. The misalignment is due to several reasons, including buoyancy and catalytic effect of the thermocouple, which are not included in the model. As discussed by Seiser et al. [20], who also reported a similar shift, fuel issues from the bottom nozzle, and being a denser fluid, it pushes the lighter hot-flame-zone gases upward. This causes a small rightward shift in temperature and concentration profiles toward the oxidizer nozzle, as indicated in Fig. 3.

Our quartz microprobe has very small dimensions that minimize disturbances to the flowfield. Thus, the measured species-concentration profiles are well reproduced by the model (in Fig. 3) for all the major reactant and product species and intermediate species such as CO and H_2. The agreement between predictions and experimental data is also quite good for intermediate hydrocarbon species (CH_4, C_2H_4, C_2H_2, and C_3H_x). Discrepancies are usually in the range of measurement uncertainties. The good agreement between the predicted and measured nitrogen concentration profiles for both flames indicates that species transport is reasonably well reproduced in the simulations.

Flames A1 and B1 have similar structure, although flame B1 is spatially wider, due to its lower strain rate. For both flames, there is a single nonpremixed reaction zone on the oxidizer side of the stagnation plane, as indicated by the temperature and velocity profiles. As expected, the locations of the CO and H_2 concentration peaks precede those of the CO_2 and H_2O concentration peaks[†]. All of these peaks are located in the high-temperature region. On the other hand, the C_2- and other intermediate hydrocarbon species have maximum concentrations on the fuel side of the flame, on which pyrolysis occurs [37]. The profiles for flame A1 exhibit sharper peaks because of the higher strain rate. The effect of nitrogen dilution can be seen in the peak temperature values. The flame-A1 peak temperature is 1798 K, and flame-B1 peak temperature is 1933 K, both values being much lower than the adiabatic-flame temperature (2274 K) of n-heptane/air mixture.

To characterize the effect of strain rate on the flame structure, we now discuss measurements and simulations for two other n-heptane/air nonpremixed flames. Figure 4 presents temperature, velocity, and species mole fraction profiles for flames A2 and A3, corresponding to strain rates of 100 and 50 s^{-1}, respectively. These cases, together with flame A1, are all relatively close to extinction, due to large nitrogen dilutions (ranging from 85 to 90%) of the fuel stream. There is also generally good agreement between measured and numerical data for these two flames, especially for temperature and major reactant and product species. Flame A3 is spatially broader than flame A2, due to the lower strain rate. The buoyant misalignment between measurements and predictions for it is larger than for flames A1 and A2, which provides evidence of the stronger buoyancy effect at low strain-rate values.

The peaks in the profiles of the C_3 species ethylene, acetylene, and methane are influenced by the strain rate, because it has an

[†]For clarity, different x scales were used for some of the species profiles.

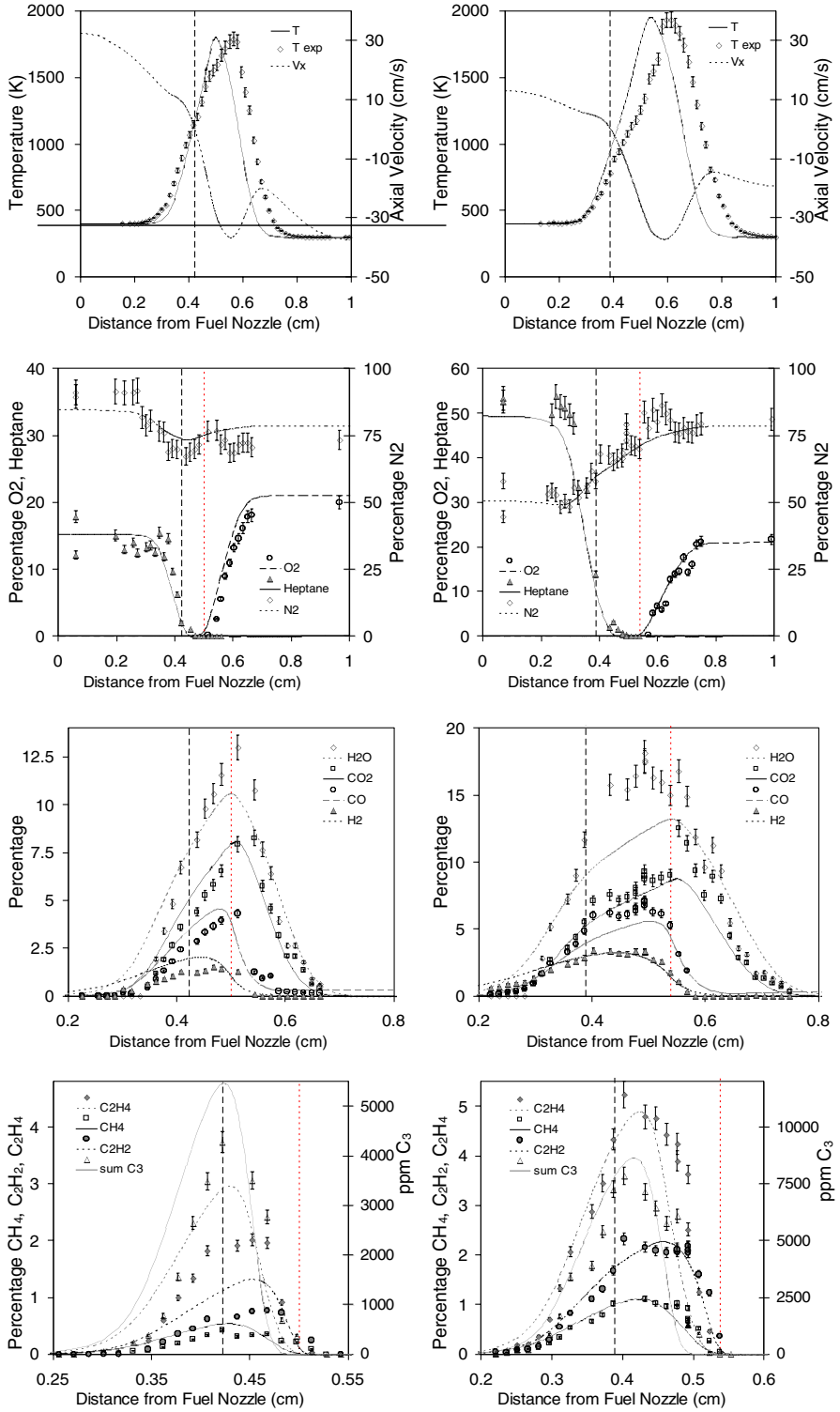

Fig. 3 Predicted (lines) and measured (symbols) profiles for flames A1 (left) and B1 (right); temperature, axial velocity, and mole fraction profiles of O_2, N_2, n-C_7H_{16}, H_2O, CO_2, CO, H_2, CH_4, ethylene, acetylene and C_3 hydrocarbons; vertical lines in some figures indicate the locations of the stagnation plane and the peak temperature.

effect on the stagnation-plane location relative to the hot region and the peak temperature. The peaks for these species lie near the stagnation plane, on which the residence time is relatively large. Going from flame A1 to flame A3, the separation between the stagnation plane and the peak temperature increases because the strain rate decreases, whereas the peak temperature decreases because the dilution of the fuel stream increases and the radiative heat loss increases at lower strain rates. Because this reduces the rate of heat transport from the flame toward the stagnation plane, pyrolysis reactions are diminished.

A major objective of this work is to characterize the relative soot formation in n-heptane flames through the formation of major soot precursors such as acetylene and benzene, which lie along the growth process to PAH. Figures 2 and 3 indicate that flame B1 is sooting, whereas flame A1 is nearly nonsooting. However, both the predictions and measurements provide evidence that soot-precursor pathways are important for both cases. The measured and predicted profiles of acetylene and benzene mole fractions are presented in Figs. 3–5. The acetylene profiles for flames A1, B1, A2, and A3 are contained in Figs. 3 and 4, and those of benzene are shown in Fig. 5.

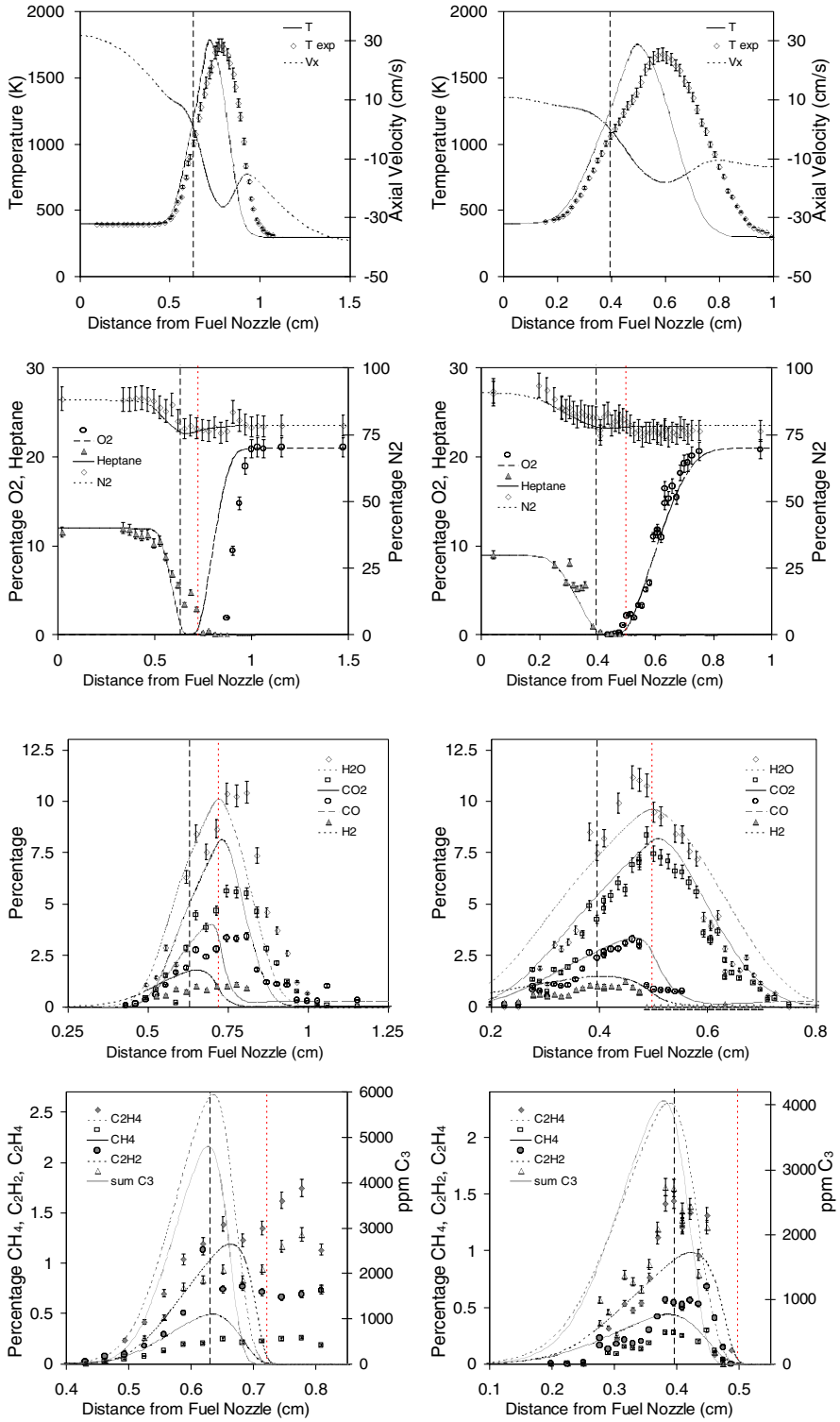

Fig. 4 Predicted (lines) and measured (symbols) profiles for flames A2 (left) and A3 (right); temperature, axial velocity, and mole fraction profiles of O_2, N_2, n-C_7H_{16}, H_2O, CO_2, CO, H_2, CH_4, ethylene, acetylene and C_3 hydrocarbons; vertical lines in some figures indicate the locations of the stagnation plane and the peak temperature.

The measured and predicted acetylene profiles are in agreement with each other and with results from other investigators, but benzene measurements in n-heptane counterflow nonpremixed flames have not been previously reported, and so a definitive comparison could not be made. The predictions are unable to reproduce the measured benzene profiles. We also observed a similar disagreement between the measurements and prediction for benzene in n-heptane/air counterflow partially premixed flames [22,26]. Benzene mole fractions have also been measured by El Bakali et al. [41] in a laminar premixed flame.

To examine these discrepancies further, the dominant reactions associated with benzene formation were identified through a pathway analysis. Results are summarized in Fig. 6 and Table 2. Figure 6a shows the most important pathways of benzene formation in flame A1 at a location corresponding to the peak benzene mole fraction (0.428 cm from the fuel nozzle). The kinetic rates of the dominant reactions are listed in Table 2. The most important formation pathway is the recombination of propargyl radicals to form either benzene (R1) or phenyl (R2). The most important reaction for the formation of propargyl radical is the H abstraction on propadiene

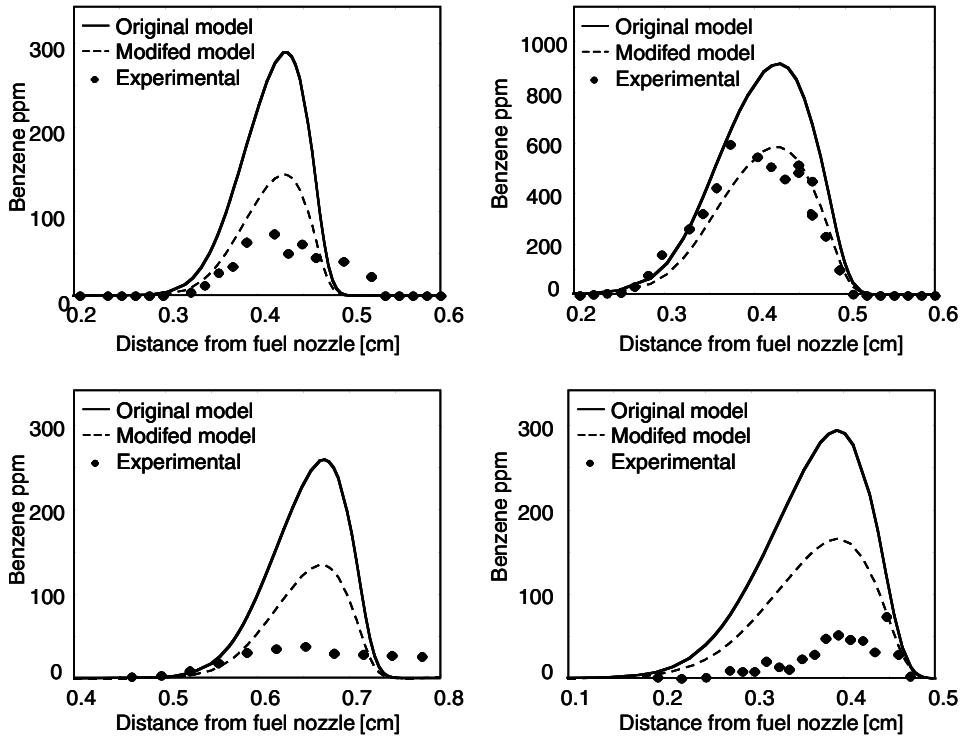

Fig. 5 Predicted (lines) and measured (symbols) benzene profiles for flames A1 (top left), B1 (top right), A2 (bottom left), and A3 (bottom right); predictions are based on the original and modified mechanisms.

(R3), which is formed from the reaction of allyl radical C_3H_5 with H (R4). Other pathways of benzene formation are the reaction between C_2 and C_4 species and that of toluene with H. Toluene is formed by the recombination and H-abstraction reactions of benzyl radical, which is formed by phenyl and also by C_2H_2 and cyclopentadienyl. The only significant consumption pathway of benzene is the H-abstraction reaction to form phenyl, which reacts with acetylene to form phenylacetylene as a first step of the well-known HACA mechanism [33]. A similar analysis was also performed at $x = 0.46$ cm from the fuel nozzle, where the temperature is higher. At this location, the interactions between C_2 and C_4 species are not important anymore, whereas the recombination of propargyl radicals becomes more important.

The dominant pathways of benzene formation in flame B1 are shown in Fig. 6b. Both the temperatures and benzene peak locations are similar in flames A1 and B1. Although all the reactions associated with benzene formation have noticeably higher rates in flame B1 (due to higher fuel concentration) than those in flame A1, the relative importance of the different pathways is quite similar; that is, the recombination of propargyl is the most important reaction, but the interactions between C_2 and C_4 also have an significant impact on the formation of benzene. At 0.495 cm from the fuel nozzle, only the C_3 pathway is important, and the reaction of toluene with H is less important. For this case, toluene is formed by phenyl and by the reaction of propargyl with C_4H_4, whereas the reaction of C_2H_2 with cyclopentadiene occurs in the reverse direction (i.e., it consumes toluene). At this location, the oxidation reactions of benzene start to become important. In particular, benzene is consumed not only by H abstraction, but also by reaction with OH to form cyclopentadienyl or phenol.

The results of the sensitivity analysis indicate that reaction 4 (see Table 2) has the strongest influence on benzene formation. Although the C_3H_4 concentration measurement could have provided useful information regarding the accuracy of the reaction rate constants for this reaction, the gas-chromatograph sampling technique could not resolve all of the C_3– hydrocarbons. The kinetic parameters reported by Tsang [42] for reaction 4 are about four times lower than those contained in the original mechanism (see Table 2). Benzene predictions in the four flames with Tsang's kinetic parameter are compared in Fig. 5 with the experimental measurements and the predictions of the original mechanism. The improvement in the predicted benzene profile is evident for all four flames. In the relatively less sooting flames (i.e., flames A1, A2, and A3), the predicted benzene is still high, but significantly better, whereas in flame B1, the prediction becomes very good within experimental uncertainties. Only the C_6H_6 mole fraction profiles are shown with the modified mechanism, because no differences were observed for the temperature and the other species profiles. It is important to note that in the laminar premixed flame of El Bakali et al. [41], the predicted benzene profile using the modified mechanism also shows better agreement with the measured profile.

Table 2 Dominant reactions associated with benzene formation

	Reaction	A, [a]	β, [a]	E_a, [a]	Reference
1	$C_3H_3 + C_3H_3 \rightarrow C_6H_6$	3.0×10^9	0	0	Ranzi et al. [28]
2	$C_3H_3 + C_3H_3 \rightarrow C_6H_5 + H$	3.0×10^9	0	0	Ranzi et al. [28]
3	$OH + CH_2 = C = CH_2 \rightarrow H_2O + C_3H_3$	2.0×10^4	2	1000	Ranzi et al. [28]
	$H + CH_2 = C = CH_2 \rightarrow H_2 + C_3H_3$	5.0×10^4	2	5000	Ranzi et al. [28]
	$CH_3 + CH_2 = C = CH_2 \rightarrow CH_4 + C_3H_3$	4.0×10^{10}	0	16,000	Ranzi et al. [28]
4	$H + CH - CH - CH_2 \rightarrow H_2 + CH_2 = C = CH_2$	1.81×10^{10}	0	0	Tsang [42]

[a]Three-parameter form of the Arrhenius equation $k(T) = AT^{\beta} \exp(-E_a/RT)$; units are kmol, m^3, kcal, and K

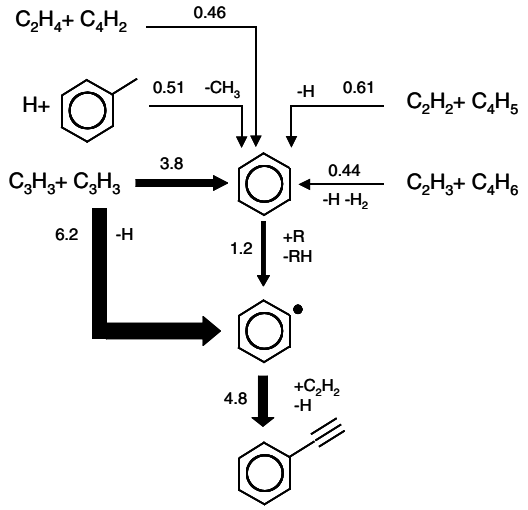

a)

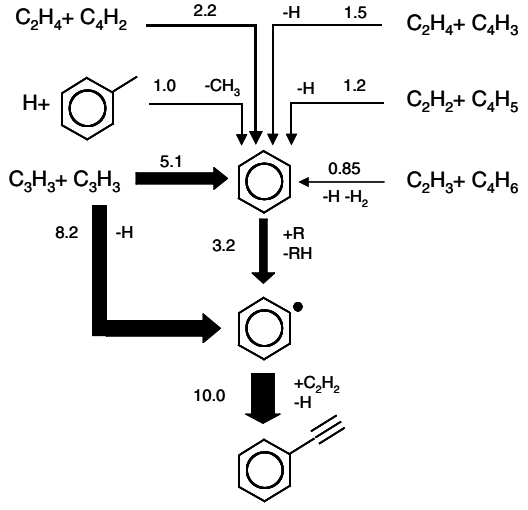

b)

Fig. 6 Main pathways of benzene formation and consumption in a) flames A1 and b) B1 at 0.429 cm from the fuel nozzle; thickness of the arrows is proportional to the reaction rate; numbers are the reaction rates times 10^4 kmol/m^3/s.

Conclusions

An experimental and numerical investigation was performed to examine the structure and emission characteristics of N_2-diluted nonpremixed n-heptane/air counterflow flames. Well-resolved experimental data for temperature and species-concentration profiles, including those of major species (n-heptane, O_2, N_2, CO, H_2, CO_2, and H_2O), intermediate hydrocarbon species (CH_4, C_2H_4, C_2H_2, and C_3H_x), and aromatic species (C_6H_6) have been reported for prevaporized n-heptane counterflow flames established at different levels of nitrogen dilution and strain rate. The measurements have been compared with simulations performed using a comprehensive reaction mechanism that includes detailed chemistry models for n-heptane oxidation and NOx and PAH species (up to $C_{24}H_{12}$) formation. Based on this comparison, the mechanism was modified to better predict the pyrolysis reactions associated with the formation of PAH species.

There is good quantitative agreement between measurements and predictions for temperature, major reactant/product species (n-heptane, O_2, N_2, and CO_2), and intermediate fuel species (H_2 and CO). There is also a fairly good agreement for intermediate hydrocarbon species (CH_4, C_2H_4, C_2H_2, and C_3H_x) as well as for benzene. For the conditions investigated, the reaction pathways analysis indicate that the major benzene formation reaction is the recombination of propargyl radicals, whereas the important reaction for the formation of propargyl radical is the H abstraction on propadiene, which is formed from the reaction of allyl radical C_3H_5 with H. Other pathways of benzene formation are the reaction between C_2 and C_4 species and that of toluene with H. Toluene is formed by the recombination and H-abstraction reactions of benzyl radical, which is formed by phenyl and also by C_2H_2 and cyclopentadienyl. The consumption of benzene occurs mainly through the H-abstraction reaction to form phenyl, which reacts with acetylene to form phenylacetylene as a first step of the well-known HACA mechanism.

References

[1] Westbrook, K., and Dryer, F. L., "Chemical Kinetic Modeling of Hydrocarbon Combustion," *Progress in Energy and Combustion Science*, Vol. 10, No. 1, 1984, pp. 1–57. doi:10.1016/0360-1285(84)90118-7

[2] Card, J. M., and Williams, F. A., "Asymptotic Analysis with Reduced Chemistry for the Burning of n-Heptane Droplets," *Combustion and Flame*, Vol. 91, No. 2, 1992, pp. 187–199. doi:10.1016/0010-2180(92)90099-B

[3] Bolling, M., Pitsch, H., Hewson, J., and Seshadri, K., "Reduced n-Heptane Mechanism for Non-Premixed Combustion with Emphasis on Pollutant-Relevant Intermediate Species,"*Proceedings of the Combustion Institute*, Vol. 26, 1996, pp. 729–737.

[4] Li, S. C., Libby, P. A., and Williams, F. A., *Proceedings of the Combustion Institute*, Vol. 24, Combustion Inst., Pittsburgh, PA, 1992, pp. 1503–1512.

[5] Bui, M., and Seshadri, K., "Comparison Between Experimental Measurements and Numerical Calculations of the Structure of Heptane-Air Diffusion Flames," *Combustion Science and Technology*, Vol. 79, Nos. 4–6, 1991, pp. 293–310. doi:10.1080/00102209108951771

[6] Chelliah, H. K., Bui-Pham, M., Seshadri, K., and Law, C. K., *Proceedings of the Combustion Institute*, Vol. 24, Combustion Inst., Pittsburgh, PA, 1992, pp. 851–857.

[7] Lindstedt, R. P., and Maurice, L. Q., "Detailed Kinetic Modelling of n-Heptane Combustion," *Combustion Science and Technology*, Vol. 107, Nos. 4–6, 1995, pp. 317–353. doi:10.1080/00102209508907810

[8] Held, T. J., Marchese, A. J., and Dryer, F. L., "A Semi-Empirical Reaction Mechanism for n-Heptane Oxidation and Pyrolysis," *Combustion Science and Technology*, Vol. 123, Nos. 1–6, 1997, pp. 107–146. doi:10.1080/00102209708935624

[9] Zeppieri, S. P., Klotz, S. D., and Dryer, F. L., *Proceedings of the Combustion Institute*, Vol. 28, Combustion Inst., Pittsburgh, PA, 2000, pp. 1587–1596.

[10] Seiser, R., Pitch, H., Seshadri, K., Pitz, W. J., and Curran, H. J., "Extinction and Autoignition of n-Heptane in Counterflow Configuration," *Proceedings of the Combustion Institute*, Vol. 28, Combustion Inst., Pittsburgh, PA, 2000, pp. 2029–2037.

[11] Curran, H. J., Gaffuri, P., Pitz, W. J., and Westbrook, C. K., "A Comprehensive Modeling Study of n-Heptane Oxidation," *Combustion and Flame*, Vol. 114, Nos. 1–2, 1998, pp. 149–177. doi:10.1016/S0010-2180(97)00282-4

[12] Ranzi, E., Gaffuri, P., Faravelli, T., and Dagaut, P., "A Wide-Range Modeling Study of n-Heptane Oxidation," *Combustion and Flame*, Vol. 103, Nos. 1–2, 1995, pp. 91–106. doi:10.1016/0010-2180(95)00091-J

[13] Chakir, A., Belliman, M., Boettner, J. C., and Cathonnet, M., "Kinetic Study of n-Heptane Oxidation," *International Journal of Chemical Kinetics*, Vol. 24, No. 4, 1992, pp. 385–410. doi:10.1002/kin.550240407

[14] Kent, H. J., and Williams, F. A., "Extinction of Laminar Diffusion Flames for Liquid Fuels," *Proceedings of the Combustion Institute*, Vol. 15, 1974, pp. 315–325.

[15] Hamins, A., and Seshadri, K., "The Structure of Diffusion Flames Burning Pure, Binary, and Ternary Solutions of Methanol, Heptane, and Toluene," *Combustion and Flame*, Vol. 68, No. 3, 1987, pp. 295–307. doi:10.1016/0010-2180(87)90006-X

[16] Hamins, A., Trees, D., Seshadri, K., and Chelliah, H. K., "Extinction of Nonpremixed Flames with Halogenated Fire Suppressants," *Combustion and Flame*, Vol. 99, No. 2, 1994, pp. 221–230. doi:10.1016/0010-2180(94)90125-2

[17] Abdel-Khalik, S. I., Tamaru, T., and El-Wakil, M. M., "Chromatographic an Interferometric Study of the Diffusion Flame Around a Simulated Drop," *Proceedings of the Combustion Institute*, Vol. 15, Combustion Inst., Pittsburgh, PA, 1974, pp. 389–399.

[18] Nayagam, V., Haggard, J. B., Jr., Colantonio, R. O., Marchese, A. J., Dryer, F. L., and Williams, F. A., "Microgravity n-Heptane Droplet Combustion in Oxygen-Helium Mixtures at Atmospheric Pressure," *AIAA Journal*, Vol. 36, No. 8, 1998, pp. 1369–1378.

[19] Gibbs, G. J., and Calcote, H. F., "Effect of Molecular Structure on Burning Velocity," *Journal of Chemical and Engineering Data*, Vol. 4, 1959, pp. 226–237.

[20] Seiser, R., Truett, L., Trees, D., and Seshadri, K., "Structure and Extinction of Non-Premixed n-Heptane Flames," *Proceedings of the Combustion Institute*, Vol. 27, Combustion Inst., Pittsburgh, PA, 1998, pp. 649–657.

[21] Li, S. C., and Williams, F. A., "Counterflow Heptane Flame Structure," *Proceedings of the Combustion Institute*, Vol. 28, Combustion Inst., Pittsburgh, PA, 2000, pp. 1031–1038.

[22] Berta, P., Puri, I. K., and Aggarwal, S. K., "Structure of Partially Premixed n-Heptane–Air Counterflow Flames," *Proceedings of the Combustion Institute*, Vol. 30, Combustion Inst., Pittsburgh, PA, 2005, pp. 447–453.
doi:10.1016/j.proci.2004.08.141

[23] Oberdörster, G., "Pulmonary Effects of Inhaled Ultrafine Particles," *International Archives of Occupational and Environmental Health*, Vol. 74, No. 1, 2001, pp. 1–8.

[24] Frenklach, M., Clary, D. W., Gardiner, W. C., and Stein, S. E., "Detailed Kinetic Modeling of Soot Formation in Shock-Tube Pyrolysis of Acetylene," *Proceedings of the Combustion Institute*, Vol. 20, Combustion Inst., Pittsburgh, PA, 1985, pp. 887–903.

[25] Dente, M., Ranzi, E., and Goossens, A. G., "Detailed Prediction of Olefin Yields from Hydrocarbon Pyrolysis Through a Fundamental Simulation Model (SPYRO)," *Computers and Chemical Engineering*, Vol. 3, Nos. 1–4, 1979, pp. 61–75.
doi:10.1016/0098-1354(79)80013-7

[26] Berta, P., Puri, I. K., and Aggarwal, S. K., "An Experimental and Numerical Investigation of n-Heptane/Air Counterflow Partially Premixed Flames and Emission of NOx and PAH Species," *Combustion and Flame*, Vol. 145, No. 4, 2006, pp. 740–764.
doi:10.1016/j.combustflame.2006.02.003

[27] Liu, S., Hewson, J. C., Chen, J. H., and Pitsch, H., "Effects of Strain Rate on High-Pressure Nonpremixed n-Heptane Autoignition in Counterflow," *Combustion and Flame*, Vol. 137, No. 3, 2004, pp. 320–339.
doi:10.1016/j.combustflame.2004.01.011

[28] Ranzi, E., Dente, M., Goldaniga, A., Bozzano, G., and Faravelli, T., "Lumping Procedures in Detailed Kinetic Modeling of Gasification, Pyrolysis, Partial Oxidation and Combustion of Hydrocarbon Mixtures," *Progress in Energy and Combustion Science*, Vol. 27, No. 1, 2001, p. 99.
doi:10.1016/S0360-1285(00)00013-7

[29] Faravelli, T., Goldaniga, A., and Ranzi, E., "The Kinetic Modeling of Soot Precursors in Ethylene Flames," *Proceedings of the Combustion Institute*, Vol. 27, Combustion Inst., Pittsburgh, PA, 1998, pp. 1489–1495.

[30] Frassoldati, A., Faravelli, T., and Ranzi, E., "Kinetic Modeling of the Interactions Between NO and Hydrocarbons at High Temperature," *Combustion and Flame*, Vol. 135, Nos. 1–2, 2003, pp. 97–112.
doi:10.1016/S0010-2180(03)00152-4

[31] Puri, I. K., and Seshadri, K., "Extinction of Diffusion Flames Burning Diluted Methane and Diluted Propane in Diluted," *Combustion and Flame*, Vol. 65, No. 2, 1986, pp. 137–150.
doi:10.1016/0010-2180(86)90015-5

[32] Goldaniga, A., Faravelli, T., and Ranzi, E., "The Kinetic Modeling of Soot Precursors in a Butadiene Flame, *Combustion and Flame*, Vol. 122, No. 3, 2000, pp. 350–358.
doi:10.1016/S0010-2180(00)00138-3

[33] Wang, H., and Frenklach, M., "A Detailed Kinetic Modeling Study of Aromatics Formation in Laminar Premixed Acetylene and Ethylene Flames," *Combustion and Flame*, Vol. 110, Nos. 1–2, 1997, pp. 173–221.
doi:10.1016/S0010-2180(97)00068-0

[34] Xu, F., El-Leathy, A. M., Kim, C. H., and Faeth, G. M., "Soot Surface Oxidation in Hydrocarbon/Air Diffusion Flames at Atmospheric Pressure," *Combustion and Flame*, Vol. 132, Nos. 1–2, 2003, pp. 43–57.
doi:10.1016/S0010-2180(02)00459-5

[35] Lutz, A. E., Kee, R. J., Grcar, J. F., and Rupley, F. M., "OPPDIF: A FORTRAN Program for Computing Opposed Flow Diffusion Flames," Sandia National Labs., Rept. SAND96-8243, Albuquerque, NM, 1997.

[36] Pogliani, B., Bundy, M., Hamins, A., and Puri, I. K., "Thermal Radiation Effects on the Extinction of Inhibited Flames," 2nd Joint Technical Meeting of the U.S. Sections of the Combustion Institute, Combustion Inst. Paper 218, Mar. 2001.

[37] Xue, H. S., and Aggarwal, S. K., "NOx Emissions in n-Heptane/Air Partially Premixed Flames," *Combustion and Flame*, Vol. 132, No. 4, 2003, pp. 723–741.
doi:10.1016/S0010-2180(02)00534-5

[38] Burcat, A., and McBride, B., "1997 Ideal Gas Thermodynamic Data for Combustion and Air-Pollution Use," Technion—Israel Inst. of Technology, Rept. TAE 804, Haifa, Israel, 1997.

[39] Benson, S. W., *Thermochemical Kinetics*, 2nd ed., Wiley, New York, 1976.

[40] Kee, R. J., Dixon-Lewis, G., Warnatz, J., Coltrin, M. E., and Miller, J. A., "A FORTRAN Computer Code Package for the Evaluation of Gas-Phase Multicomponent Transport Properties," Sandia National Labs., Rept. SAND86-8246, Albuquerque, NM, 1986.

[41] El Bakali, A., Delfau, J.-L., and Vovelle, C., "Experimental Study of 1 Atmosphere, Rich, Premixed n-Heptane and Iso-Octane Flames," *Combustion Science and Technology*, Vol. 140, Nos. 1–6, 1998, p. 69.
doi:10.1080/00102209808915768

[42] Tsang, W., "Chemical Kinetic Data Base for Combustion Chemistry, Part 5: Propene," *Journal of Physical and Chemical Reference Data*, Vol. 20, 1991, pp. 221–273.

C. Avedisian
Associate Editor